# X-ray Diffractive Imaging of Highly Ionized Helium Nanodroplets

Alexandra J. Feinberg<sup>1</sup>, Felix Laimer<sup>2</sup>, Rico Mayro P. Tanyag<sup>3</sup>, Björn Senfftleben<sup>4,5</sup>, Yevheniy Ovcharenko<sup>4</sup>, Simon Dold<sup>4</sup>, Michael Gatchell<sup>2,6</sup>, Sean M.O. O'Connell-Lopez<sup>1</sup>, Swetha Erukala<sup>1</sup>, Catherine A. Saladrigas<sup>7,8</sup>, Benjamin W. Toulson<sup>7</sup>, Andreas Hoffmann<sup>5</sup>, Ben Kamerin<sup>9</sup>, Rebecca Boll<sup>4</sup>, Alberto De Fanis<sup>4</sup>, Patrik Grychtol<sup>4</sup>, Tommaso Mazza<sup>4</sup>, Jacobo Montano<sup>4</sup>, Kiana Setoodehnia<sup>4</sup>, David Lomidze<sup>4</sup>, Robert Hartmann<sup>10</sup>, Philipp Schmidt<sup>4</sup>, Anatoli Ulmer<sup>3</sup>, Alessandro Colombo<sup>11</sup>, Michael Meyer<sup>4</sup>, Thomas Möller<sup>3</sup>, Daniela Rupp<sup>5,11\*</sup>, Oliver Gessner<sup>7\*</sup>, Paul Scheier<sup>2\*</sup>, Andrey F. Vilesov<sup>1,9\*</sup>.

<sup>1</sup>Department of Chemistry, University of Southern California, Los Angeles, California USA.

<sup>2</sup>Department of Physics, Universität Innsbruck, Innsbruck, Austria.

<sup>3</sup>Institut für Optik und Atomare Physik, Technische Universität Berlin, Germany.

<sup>4</sup>European X-ray Free Electron Laser, Schenefeld, Germany.

<sup>5</sup>Max-Born Institut for Nonlinear Optics and Short Pulse Spectroscopy, Berlin, Germany.

<sup>6</sup>Department of Physics, Stockholm University, Stockholm, Sweden.

<sup>7</sup>Chemical Sciences Division, Lawrence Berkeley National Laboratory. Berkeley, California, USA.

<sup>8</sup>Department of Chemistry, University of California Berkeley, California, USA.

<sup>9</sup>Department of Physics and Astronomy, University of Southern California, Los Angeles, California, USA.

<sup>10</sup>PNSensor GmbH, München, Germany.

<sup>11</sup>Laboratory for Solid State Physics, ETH Zurich, Zurich, Switzerland.

\*Corresponding authors. Emails: ruppda@phys.ethz.ch, ogessner@lbl.gov, paul.scheier@uibk.ac.at, vilesov@usc.edu.

#### Abstract

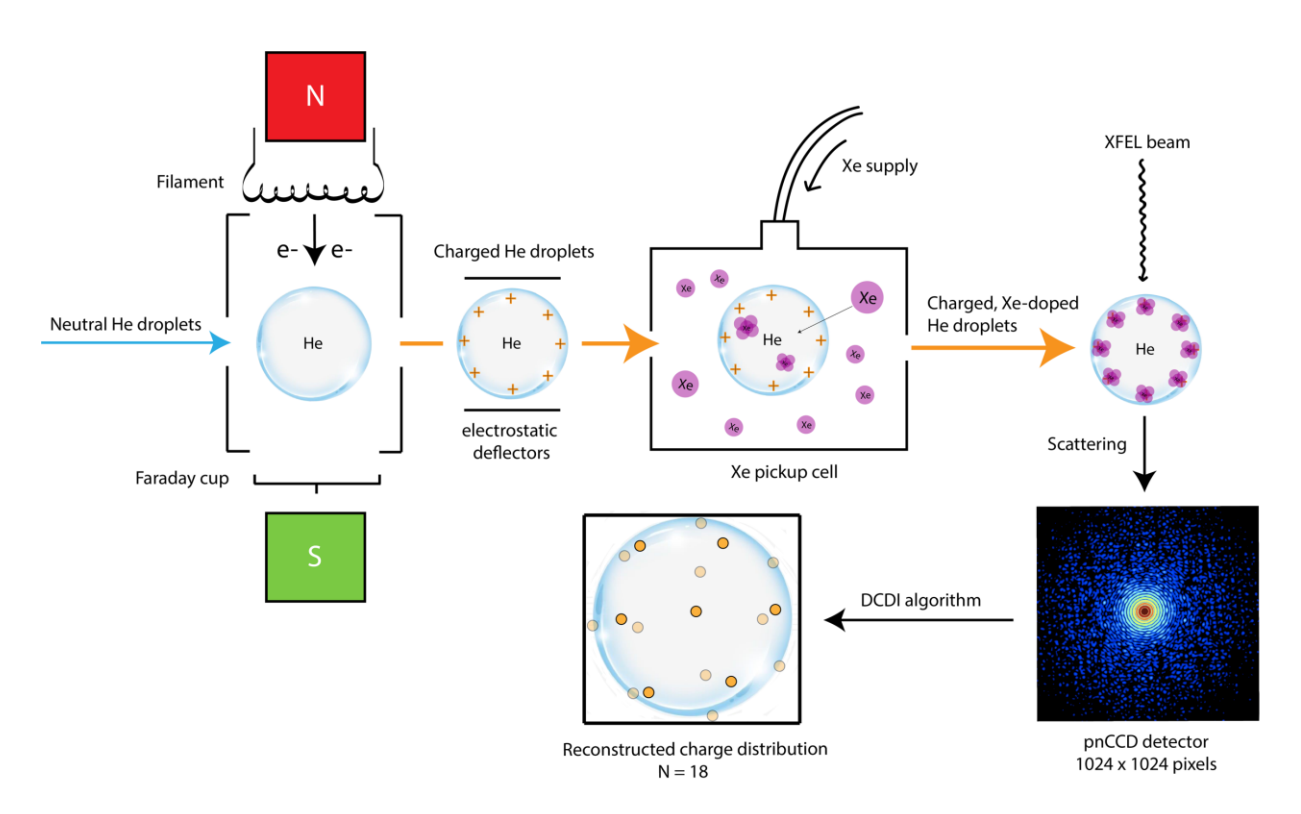
Finding the lowest energy configuration of N unit charges on a sphere, known as Thomson's problem, is a long-standing query which has only been studied via numerical simulations. We present its physical realization using multiply charged He nanodroplets. The charge positions are determined by x-ray coherent diffractive imaging with Xe as a contrast agent. In neutral droplets, filaments resulting from Xe atoms condensing on quantum vortices are observed. Unique to charged droplets, however, Xe clusters that condense on charges are distributed on the surface in lattice-like structures, introducing He droplets as experimental model systems for the study of Thomson's problem.

In 1904, J.J. Thomson sought to find the configuration of N unit charges on a sphere that minimizes the overall Coulombic energy (1). A related problem of packing particles on a sphere has since appeared in the research of highly ordered finite systems such as viral morphology, crystallography, and molecular structure (2-5). Generally, Thomson's problem remains unsolved, though numerical simulations have yielded a variety of configurations depending on the number of charges. Locally, calculations yield charge distributions characterized by triangular lattice configurations with ~6 nearest neighbors per charge (6-12). Surprisingly, it has been shown that the minimum energy configuration isn't always the one that places the charges at furthest distance from each other, nor the configuration with greatest symmetry.

It isn't immediately clear if an idealized Thomson problem that ignores the roles of thermal or quantum mechanical kinetic energies has any practical significance. However, charged submicrometer helium droplets present an extraordinary experimental realization (10) because they remain liquid down to absolute zero temperature and can hold hundreds of charges, which are effectively confined and pushed to the droplet's surface due to their mutual Coulomb repulsion. Surface liquid helium acts as a suitable support to study the structure and collective properties of two-dimensional Coulomb systems, i.e., those made of electrons or cations (13-16). Closely related to the Thomson problem are electrons inside multielectron bubbles in liquid helium which were discussed as model systems to study the electronic structure of two-dimensional gases of electrons on a sphere with substantial ripplon coupling (17). A very recent study reports stable bubbles containing 6 and 8 electrons (18). However, the study of multielectron bubbles is hindered by dynamic instability and their irregular shape (19, 20).

It is inevitable that a physical realization of the Thomson problem differs from its purely mathematical cousin in some important respects. Exact localization of charges on a sphere is physically untenable because it requires infinite potentials. Pursuant to a helium droplet, the charges are held within the droplet by some finite solvation potential. Therefore, their radial positions can vary to some extent. The surface tension of liquid helium is rather small, which may result in some local surface deformation. Some departure from a spherical shape may also be caused by droplet's rotation. It would therefore be very interesting see the effect of the physical modalities on the configuration, which has so far been only studied in terms of an abstract mathematical model.

Recently, Laimer et al. demonstrated that multiply charged <sup>4</sup>He droplets can be produced via electron impact (21). The cations in He droplets likely exist in the form of a covalently bound He<sub>3</sub><sup>+</sup> units, which are formed within less than 10 ps from He<sup>+</sup> ions that initially produced upon the electron impact (22). Here, the arrangement of charges in helium droplets is studied via scattering of radiation from an x-ray free electron laser (XFEL). Visualization of charges is achieved by doping the droplets with xenon (Xe) atoms, which cluster around the charges and serve as contrast agents. The cluster positions are obtained from diffraction images using an iterative phase retrieval algorithm (23). Distinctly different from neutral helium droplets, aggregation within charged helium droplets leads to fractured dot-like patterns with compact spots of Xe clusters throughout the droplets. We assign the compact dots to charged Xe clusters near the droplet surface.

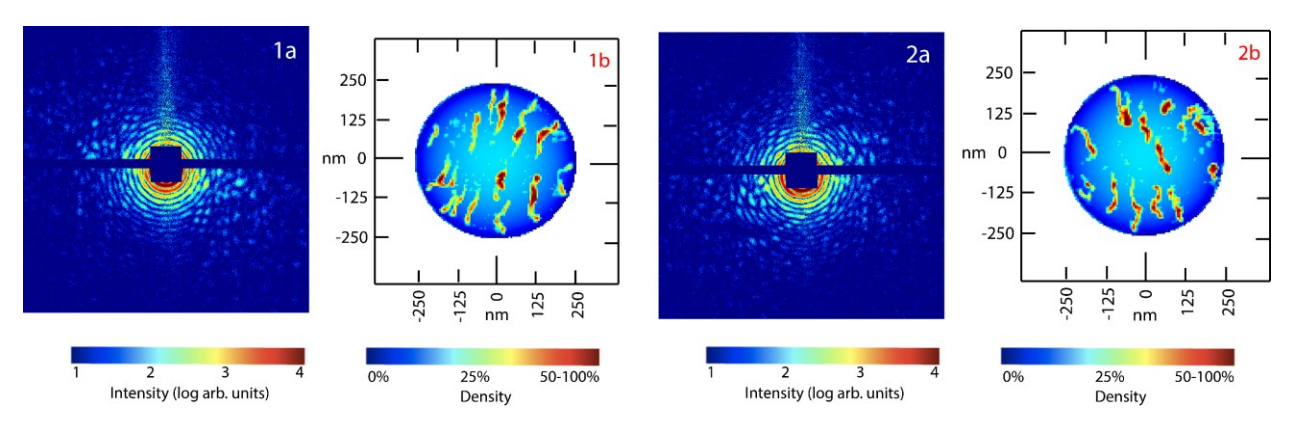


<u>Fig. 1.</u> Schematic of the experiment. Helium droplets are ionized via electron impact and pass through plane capacitor electrostatic deflectors. Ionized helium droplets are doped with Xe atoms which cluster around the positions of the charges and serve as markers. The droplets are interrogated with the XFEL. Diffraction patterns are recorded on a pnCCD detector and processed using a phase retrieval algorithm to obtain the density profile and charge distributions. The predicted configuration for 18 charges is used as an example to simulate the displayed diffraction pattern.

The experiments are performed at the Small Quantum Systems (SQS) instrument of the European XFEL (24, 25) using the Nano-sized Quantum Systems (NQS) end station. A schematic is shown in Fig. 1. Neutral helium droplets are produced via cryogenic nozzle beam expansion of

pressurized helium gas through a 5  $\mu$ m nozzle into vacuum (26). The droplets are ionized by an electron gun operating at 40 – 100 eV acceleration voltage and ionization currents between 5  $\mu$ A and 1.3 mA (21). Charged droplets pass through two parallel plate capacitors (each containing 2×2 cm² plates placed 2 cm apart from each other), used to verify the charging through electrostatic beam deflection. The ionized droplets are doped with Xe atoms (see Fig. 1) in a pickup cell. The focused XFEL beam (~3.5  $\mu$ m full-width-at-half-maximum, FWHM focal diameter) intersects the Xe doped helium droplets ~950 mm downstream from the droplet source. The XFEL is operated at 10 Hz with 1 FEL pulse per bunch train, a photon energy of 1.5 keV, a mean pulse energy of 3 mJ, and a nominal pulse duration of ~25 fs. Diffraction images are recorded with a 1-Mpixel pnCCD detector (1024×1024 pixels, 75×75  $\mu$ m² each) (27), centered along the XFEL beam axis 542 mm behind the interaction point. The detector consists of two separate panels (1024×512 pixels each), located above and below the x-ray beam with a central, rectangular cutout to accommodate the primary beam [19]. Each diffraction pattern is used to reconstruct the density distribution of Xe clusters within a single, isolated doped droplet (see Fig. 1) by applying an iterative phase retrieval algorithm termed Droplet Coherent Diffractive Imaging (DCDI) (23).

Diffraction images of neutral droplets are recorded for the initial droplet beam characterization and confirm that the droplets have an average radius of 250 nm (roughly 10<sup>9</sup> atoms) and an average aspect ratio (AR, major diffraction axis/minor diffraction axis) of 1.04, similar to previous conditions (28). The non-sphericity can be assigned to centrifugal deformation of rotating droplets (26, 28, 29). At low angular momenta and aspect ratios of 1< AR < 1.1, these can be described as spheroids. The flux of atoms carried by the droplets is monitored by the pressure rise in the beam dump chamber (26). Ionization of the droplets did not lead to any measurable decrease (<10%) in flux. However, the application ~100 V/cm to the parallel plate capacitors downstream from the ionizer completely extinguishes the droplet flux, demonstrating effective charging.



<u>Fig. 2.</u> Results for uncharged, Xe doped <sup>4</sup>He droplets. (1a), (2a): Diffraction patterns showing the central 600 x 600 detector pixels. The vertical streak in the upper half of the patterns is caused by stray light. (1b), (2b): Density reconstructions obtained with the DCDI algorithm.

Initial measurements are performed on neutral Xe doped droplets, see Fig. 2. The diffraction images, Fig. 2(1a) and Fig. 2(2a), exhibit rings close to the center and speckles in the outer region due to scattering off Xe clusters. Fig. 2(1b) and Fig. 2(2b) show the corresponding density reconstructions (helium is depicted in blue and Xe clusters in red/yellow) as obtained via DCDI. The Xe clusters form filaments aligned along a common direction. They are the result of Xe atoms condensing on the cores of quantum vortices, as documented in our previous works (23, 26, 29, 30).

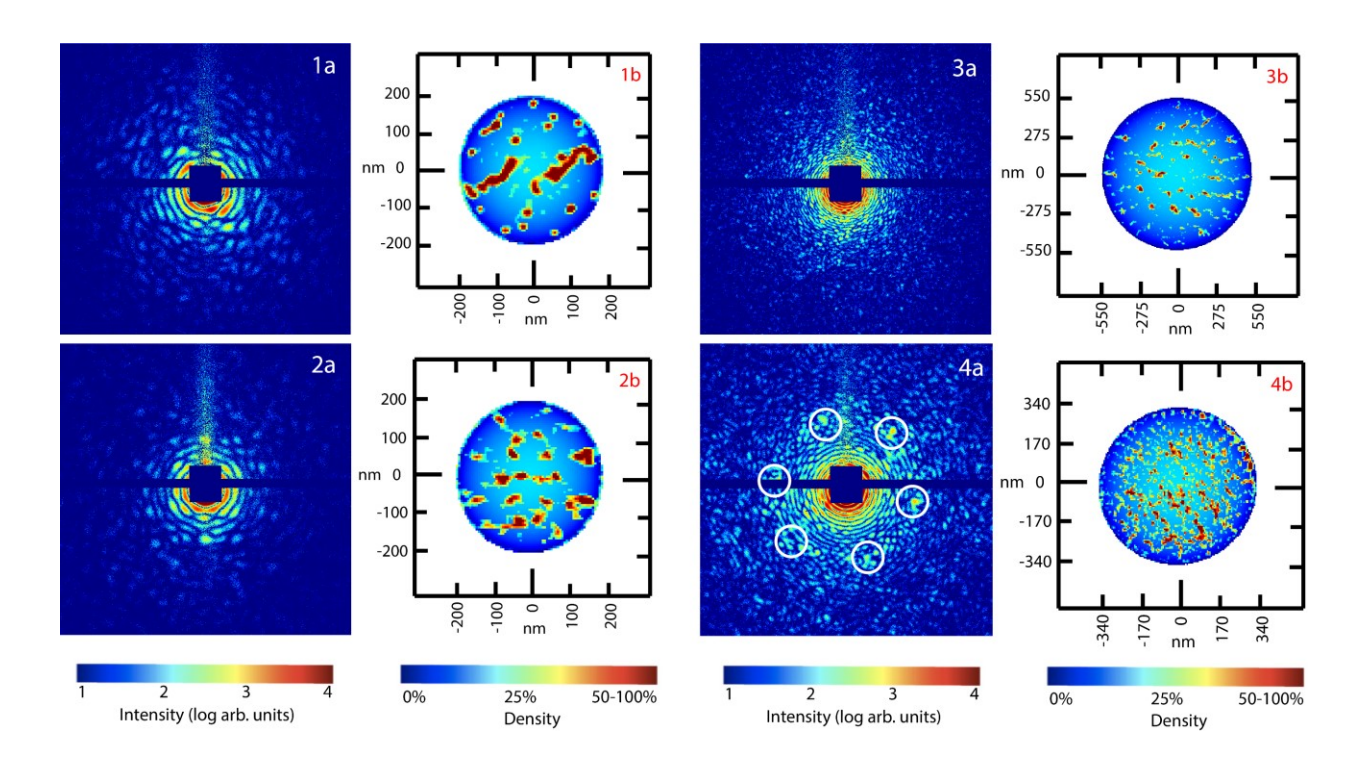


Fig. 3. Same as in Fig. 2, but for charged, Xe-doped  ${}^4\text{He}$  droplets. For droplets 1-3, the electron energy was 40 eV and emission current 30  $\mu$ A, while for droplet 4, the ionizer was set to 200 eV and 1.3 mA emission current.

Figure 3 shows diffraction patterns and density reconstructions from charged, Xe doped <sup>4</sup>He nanodroplets. The diffraction images Fig. 3(1a) – Fig. 3(3a) resemble those for uncharged droplets. Figure 3(4a) is noteworthy as it contains six Bragg spots, arranged hexagonally, which have been marked by white rings. Density reconstructions are shown in Fig. 3(1b) – Fig. 3(4b). In distinction to neutral droplets, aggregation within charged helium droplets appears unique in that it leads to fractured dot-like patterns with compact spots of Xe clusters.

The comparison of Xe densities in charged droplets (Fig. 3) with neutral droplets (Fig. 2), obtained in this work as well as in previous (23, 26, 29, 30) indicates important differences. Xe clusters in neutral droplets are seen as filaments. However, it's possible that a droplet's direction of angular momentum can be aligned with the x-ray beam such that the cylindrical vortices appear as dots on the detector plane. The coexistence, however, of dot-like features and filaments has never been observed in neutral doped droplets (23, 26, 29, 30), indicating that the dots aren't the result of a particular viewing angle. Thus, we assign the dots to the location of charged Xe clusters near the droplets' surface.

Figure 3(1b) showcases a droplet (AR = 1.02, a = 199 nm, N =  $\sim 7 \times 10^8$  helium atoms) containing two filaments and at least 16 dot-shaped clusters. The filaments primarily occupy the central volume of the droplet whereas the dots are scattered throughout the image. Figure 3(2b) shows a droplet (AR = 1.04 and a = 201 nm, N =  $\sim 7 \times 10^8$  helium atoms) with a pattern of small irregularly shaped dots. Twelve approximately equidistant Xe clusters are arranged into an ordered, oval-shaped structure. Figure 3(3b) shows a much larger droplet (AR = 1.01, a = 550 nm, N =  $\sim 10^{10}$  helium atoms) with several small clusters arranged in the center. During the experiments, droplets 1, 2, and 3 from Fig. 3 had a constant doping level, set by evaporation of  $\sim 20\%$  of the constituent helium atoms. Considering that the pickup of one Xe atom leads to evaporation of  $\sim 250$  helium atoms (26), the number of doped Xe atoms are estimated to be  $\sim 7 \times 10^5$  Xe atoms for the droplets in Fig. 3(1b) and Fig. 3(2b), and  $\sim 10^7$  Xe atoms for Fig. 3(3b) (or about  $10^{-3}$  per helium atom).

Figure 3(4b) exemplifies aggressive doping and charging conditions in larger droplets. Here, droplets were produced at nozzle settings of 60 bar, 4 K and with the ionizer set to 200 eV

and 1.3 mA emission current. The droplet (AR = 1.01, a = 337 nm, N =  $\sim 4 \times 10^9$  He atoms) in Fig. 3(4b) was doped with  $\sim 1.6 \times 10^7$  Xe atoms, leading to evaporation of  $\sim 50\%$  of helium atoms. The reconstruction shows a very dense pattern of small clusters. The details cannot be fully resolved. Note that the resolution limit of the experiment is  $\sim 20$  nm (23) or three pixels in Fig. 3(4b), whereas the average distance between the Xe clusters is estimated to be  $\sim 40$  nm.

Significant differences in the Xe density distributions upon doping neutral versus charged droplets are readily apparent. While neutrals exhibit exclusively filament-shaped Xe structures, charged droplets contain compact, dot-shaped Xe clusters often in greater numbers than the filaments. Evidently, the presence of charges influences the formation of Xe clusters. Charges in He droplets were previously proposed to serve as nucleation centers for embedded atoms (21), catalyzing the formation of clusters such as in Fig. 3(1b). The charge acquired by the droplet is estimated from the current density in the experiment ( $\sim$ 1 A/m²), time of flight of the droplet through the ionizer ( $\sim$ 25  $\mu$ s), and assuming the ionization cross section of the droplet corresponds to its geometric cross section. The estimated number of  $\sim$ 30 charges can be compared with the observed 16 dot-shaped clusters in Fig.3(1b). The agreement is reasonable considering the coarse estimate and the fact that upon creation, some charges leave the droplet in the form of He<sub>n</sub><sup>+</sup> clusters (31).

Calculations (10) show that charges in helium droplets reside close to the surface. For 20 charges, they're submerged by about 3% of the droplet radius, and move closer to the surface with increasing charge (10). Xe clusters forming around the charges increases the solvation energy, pulling the charged clusters deeper inside. Calculations (32) show that the potential energy of Xe clusters is flat in the droplet's interior but increases significantly ~10 nm from the surface. Thus, we expect charges encapsulated in Xe clusters will reside close to the surface. The distance will likely be comparable to the resolution of the present experiments of ~20 nm.

Upon doping helium droplets, vortices and surface charges compete to attract the dopants. Like other particles, some charges will be captured by vortices, while others will remain free (31, 33, 34). The partitioning depends on the droplet size, number of vortices, and the binding energy of He<sup>+</sup> to vortices. The capture impact parameter for Xe atoms by a vortex has been estimated to be  $\sim$ 0.5 nm (35), and the capture cross section of a 200 nm long filament is  $\sim$ 200 nm<sup>2</sup>. This can be compared to the cross section for the capture of a Xe atom by a charge of  $\sim$  1 nm<sup>2</sup>. This estimate assumes that He3<sup>+</sup> and Xe particles move thermally inside the He droplet and combine if their

induction interaction energy exceeds 0.38 K. Therefore, Xe atoms are mostly attracted to vortices. The situation in Fig. 3(1b) appears fortunate as only two vortices are present. However, the interpretation of Fig. 3(1b) is not straightforward, as the filaments likely contain multiple charges, the locations of which cannot be determined.

Figure 3(2b) shows an elliptic constellation of Xe clusters around the droplet center. No such structure has previously been observed in neutral droplets. The corresponding 3D structure is not obvious. For example, the figure may correspond to charged clusters attached to vortices arranged in a circle and viewed sideways, as was observed previously (30). The other Xe clusters may correspond to charges on the droplet's surface that are not attached to vortices.

Most images obtained in this work resemble that of Fig. 3(3b), exhibiting a constellation of clusters in the middle that lacks recognizable symmetry, and a small density on the periphery. Figure 3(4b) represents the extreme case of intensive charge exposure (200 eV at 1.3 mA emission current) coupled with heavy Xe doping. Although cluster configurations in Fig. 3(4b) cannot be resolved, some conclusions can be drawn from the observation of hexagonal Bragg spot arrangements in Fig. 3(4a). This pattern may originate from a system having short-range order, but lacking long-range order, such as a 2D liquid. From the spot scattering angle of about 0.021 rad, the average distance between the scattering centers is estimated to be ~40 nm. The distribution of Xe clusters at a comparable level of doping in neutral droplets (~40% of helium atoms evaporated) was previously obtained (36) and displays different features such as a network of interconnected filaments. Therefore, we assign the presence of excess Xe clusters in Fig. 3(4b) to droplet charging.

Previously observed Bragg spots in neutral droplets were assigned to lattices of quantum vortices. However, the smallest observed distance between vortices was about  $\sim 150$  nm, (26) much larger than the estimated distance between scattering centers in Fig. 3(4b). A droplet having such a tight distance between vortices will rotate at an angular velocity about two times higher than the stability threshold for droplet fission (26, 28). Assuming the scattering centers are distributed evenly (with an average distance of 40 nm) on the surface of an R = 340 nm droplet, then the number of charges is estimated to  $\sim 1000$ . In comparison, the Rayleigh criterion (10) predicts a maximum charge of 1800. It's likely that the diffraction in Fig. 3(4a) corresponds to a droplet containing a few vortices, but the formation of filaments is suppressed by aggressive charging and doping.

Small angle diffraction from a 3D object is well described by the 2D Fourier transform of the column density along the light propagation direction. For a lattice on a sphere, the projection will accurately reflect the distances between the clusters near the droplet center, but peripheral distances will appear smaller. The combined effect will be a rapid decrease in the intensity of the Bragg spots in the radial direction. This agrees with the observation of the first order Bragg spots in Fig. 3(4a). Therefore, the results in Fig. 3(4a) and Fig. 3(4b) are consistent with the Xe clusters evenly filling the surface of the droplet.

The location of charges in a spherical helium droplet was studied via Monte Carlo calculations (10), where at low T similar configurations were found as in previous calculations minimizing the potential energy (6-8, 11, 12). Melting of the charge lattice at higher temperature is characterized by a sharp increase in the number of dislocations, which in the limit of large N can be associated with the Kosterlitz–Thouless transition. The melting point corresponds to temperatures  $T^* = 0.025$  and 0.01 for N = 32 and 92 charges, respectively. Here, the dimensionless temperature,  $T^*$ , is defined as the ratio of the absolute temperature to the Coulomb energy of two elementary charges at a distance equal to the radius of the droplet. In  $^4$ He droplets  $T^* \approx 5 \times 10^{-3}$  at R = 200 nm, suggesting that a lattice could be observed in helium droplets relevant to this work.

Reconstructions from small angle scattering diffraction patterns provide coordinates of charges in the X-Y plane of the detector. The values of the Z-coordinates along the direction of the x-ray beam,  $Z = \pm \sqrt{S^2 - (X^2 + Y^2)}$ , can be obtained by assuming that all charges have the same distance S from the droplet center. The sign of Z determines if the charge resides on the front or far side of the droplet. Distinguishing charge locations on the front and far side could be achieved by finding a configuration of minimum potential energy. Currently, this approach is hindered by the presence of vortex filaments, which may also contain some charges with unknown locations. If vortices could be eliminated, the droplets will presumably only contain point-like clusters, which will contain larger numbers of xenon atoms than in the current experiment and produce correspondingly brighter diffraction signals. Our previous work (23) shows that a shift along the Z-coordinate results in a phase shift of the complex density of xenon atoms, which could be used to distinguish the locations at the two surfaces. This will provide accurate (+/-10 nm) positions of charges on the front and far sides of the droplet and close to the center. However, the reconstructed Z values for points on the peripheries of the droplet will have large uncertainties. To achieve a full 3D reconstruction, large angle scattering experiments will be needed.

In summary, charged helium droplets are a promising experimental realization of Thomson's problem for determining the minimum energy configuration of charges on a sphere. This work shows that droplets of a few hundreds of nm in radius and containing up to several hundreds of charges can be utilized as Thomson systems. While Thomson-type surface lattices of charge sites were observed, it was also discovered that quantum vortices can coexist with the charge lattice and act as dominant scavengers of Xe atoms. Nevertheless, our results indicate that quasi-free charges occupy positions near the droplet surface, forming lattice structures consistent with numerical solutions of Thomson's problem. Future experiments with <sup>3</sup>He droplets could provide opportunities to advance these studies as they are devoid of quantum vortices above ~0.15 K.

# **Data Availability Statement**

The data that support the findings of this study are stored under a proper DOI available from the corresponding authors upon reasonable request at Ref. (37).

## Acknowledgements

We acknowledge European XFEL in Schenefeld, Germany, for provision of x-ray free electron laser beam time at the SQS instrument and would like to thank the staff for their assistance. A.J.F., S.M.O.C., S.E. and A.F.V. were supported by the NSF Grant No. DMR-1701077. B.S., D.R., and A.H. acknowledge funding from the Leibniz-Gemeinschaft via grant No. SAW-2017-MBI-4. D.R. and A.C. acknowledge funding from the Swiss National Science Foundation via grant No. 200021E\_193642 and the NCCR MUST. C.A.S., B.W.T. and O.G. were supported by the Atomic, Molecular, and Optical Sciences Program of the U.S. Department of Energy, Office of Science, Office of Basic Energy Sciences, Chemical Sciences, Geosciences and Biosciences Division, through Contract No. DE-AC02-05CH11231. F.L. and P.S. were supported by the Austrian Science Fund, FWF, projects I4130 and P31149. M.G. was supported by the Swedish Research Council (contract numbers 2016-06625 and 2020-03104). T.M. was supported by DFG, project numbers 719/13 and 719/14. T.M., R.M.P.T. and A.U. acknowledge funding from the Bundesministerium für Bildung und Forschung via grant No. 05K16KT3, within the BMBF Forschungsschwerpunkt Freie-Elektronen-Laser FSP-302. This article is based upon work from

COST Action CA18212 - Molecular Dynamics in the GAS phase (MD-GAS), supported by COST (European Cooperation in Science and Technology).

## References

- 1. J. J. Thomson, On the structure of the atom: an investigation of the stability and periods of oscillation of a number of corpuscles arranged at equal intervals around the circumference of a circle; with application of the results to the theory of atomic structure. *The London, Edinburgh, and Dublin and Philosophical Magazine and Journal of Science* **6**, 237-265 (1904).
- 2. H. W. Kroto, J. R. Heath, S. C. O'Brien, R. F. Curl, R. E. Smalley, C60: Buckminsterfullerene. *Nature* **318**, 162-163 (1985).
- 3. T. Liu, E. Diemann, L. Huilin, A. W. M. Dress, A. Müller, Self-assembly in aqueous solution of wheel-shaped Mo-154 oxide clusters into vesicles. *Nature* **426**, 59-62 (2003).
- 4. R. Zandi, D. Reguera, R. F. Bruinsma, W. M. Gelbart, J. Ruddnick, Origin of icosahedral symmetry in viruses. *PNAS* **101**, 155556-115560 (2004).
- 5. H. Aranda-Espinoza *et al.*, Electrostatic Repulsion of Positively Charged Vesicles and Negatively Charged Objects. *Science* **285**, 394 (1999).
- 6. E. L. Altschuler, A. P. Garrido, Global minimum for Thomson's problem of charges on a sphere. *Phys. Rev. E* **71**, 047703 (2005).
- 7. E. L. Altschuler, T. J. Williams, E. R. Rather, F. Dowla, F. Wooten, Method of constrained global optimization. *Phys. Rev. Lett.* **72**, 2671-2674 (1994).
- 8. A. P. Garrido, M. A. Moore, Symmetric patterns of dislocations in Thomson's problem. *Phys. Rev. B* **60**, 15628-15631 (1999).
- 9. A. M. Livshits, Y. E. Lozovik, *J. Exp. and Theo. Phys.* **111**, 844-856 (2010).
- 10. A. M. Livshits, Y. E. Lozovik, Crystallization and Melting of a System of Charges in a Liquid Helium Cluster. *J. Exp. and Theo. Phys.* **105**, 571-586 (2007).
- 11. D. Mehta, J. Chen, D. Z. Chen, H. Kusumaatmaja, D. J. Wales, Kinetic Transition Networks for the Thomson Problem and Smale's Seventh Problem. *Phys. Rev. Lett.* **117**, 028301 (2016).
- 12. D. J. Wales, S. Ulker, *Phys. Rev. B* **74**, 212101 (2006).
- 13. P. Leiderer, Electrons at the surface of quantum systems. *J. Low. Temp. Phys.* **87**, 242 (1992).
- 14. P. Leiderer, Z. Phys. B. 98, 303-308 (1995).
- 15. P. Moroshkin, P. Leiderer, T. Moller, K. Kono, *Phys. Rev. E* **95**, 053110 (2017).
- 16. W. F. Vinen, C. J. Mellor, Wigner crystallization of ions trapped in superfluid 4He. *Phys. Scr.* **T35**, 145-149 (1991).
- 17. J. Tempere, I. F. Silvera, J. T. Devreese, Multielectron bubbles in helium as a paradigm for styudying electrons on surfaces with curvature. *Surf. Sci. Rep.* **62**, 159-217 (2007).
- 18. N. Yadav, P. Sen, A. Ghosh, Bubbles in superfluid helium containing six and eight electrons: Soft, quantum nanomaterial. *Sci. Adv.* **7**, eabi7128 (2021).

- 19. V. Vadakkumbatt, E. Joseph, A. Pal, A. Ghosh, Studying electrons on curved surfaces by trapping and manipulating multielectron bubbles in liquid helium. *Nat. Comm.* **5**, 4571-4576 (2014).
- 20. J. Fang, J. Tempere, I. F. Silvera, The Creation of Long-Lived Multielectron Bubbles in Superfluid Helium. *J. Low. Temp. Phys.* **187**, 54-61 (2017).
- 21. F. Laimer *et al.*, Highly Charged Droplets of Superfluid Helium. *Phys. Rev. Lett.* **123**, 165301 (2019).
- 22. M. Ovchinnikov, B. L. Grigorenko, K. C. Janda, V. A. Apkarian, Charge localization and fragmentation dynamics of ionized helium clusters. *J. Chem. Phys.* **108**, 9351-9361 (1998).
- 23. R. M. P. Tanyag *et al.*, Communication: X-ray coherent diffractive imaging by immersion in nanodroplets. *Struct Dynam-Us* **2**, 051102 (2015).
- 24. T. Tschentscher *et al.*, Photon Beam Transport and Scientific Instruments at the European XFEL. *Appl. Sci.* **7**, 592 (2017).
- 25. W. Decking *et al.*, A MHz-repetition-rate hard X-ray free-electron laser driven by a superconducting linear accelerator. *Nat. Photon.* **14**, 391-397 (2020).
- 26. L. F. Gomez *et al.*, Shapes and vorticities of superfluid helium nanodroplets. *Science* **345**, 906-909 (2014).
- 27. M. Kuster *et al.*, The 1-Megapixel pnCCD detector for the Small Quantum Systems Instrument at the European XFEL: system and operation aspects. *J. Synch. Radiat.* **28**, 576-587 (2021).
- 28. D. Verma *et al.*, Shapes of rotating normal fluid He-3 versus superfluid He-4 droplets in molecular beams. *Phys. Rev. B* **102**, 014504 (2020).
- 29. A. J. Feinberg *et al.*, Aggregation of solutes in bosonic versus fermionic quantum fluids. *Sci. Adv.* **7**, abk2247 (2021).
- 30. S. M. O. O'Connell *et al.*, Angular momentum in rotating superfluid droplets. *Phys. Rev. Lett.* **124**, 215301 (2020).
- 31. T. González-Lezana *et al.*, Solvation of ions in helium. *Int. Rev. in Phys. Chem.* **39**, 456-516 (2020).
- 32. C. Bernando, A. F. Vilesov, Kinematics of the doped quantum vortices in superfluid helium droplets. *J. Low. Temp. Phys.* **191**, 242-256 (2018).
- 33. K. R. Atkins, Ions in Liquid Helium. *Phys. Rev.* **116**, 1339-1343 (1959).
- 34. W. I. Glaberson, W. Johnson, Impurity ions in liquid helium. *J. Low. Temp. Phys.* **20**, 313-338 (1975).
- 35. I. A. Pshenichnyuk, N. A. Berloff, Inelastic scattering of xenon atoms by quantized vortices in superfluids. *Phys. Rev. B* **94**, 184505 (2016).
- 36. R. M. P. Tanyag, *Imaging Superfluid Helium Droplets, Ph. D. Thesis, University of Southern California* (2018).
- 37. A. F. Vilesov, P. Scheier, D. Rupp, O. Gessner, *EXFEL beamtime: Imaging highly charged superfluid He nanodroplets.* <a href="https://doi.org/10.22003/XFEL.EU-DATA-002714-00">https://doi.org/10.22003/XFEL.EU-DATA-002714-00</a>, (2020).